Electronic supplementary information (ESI)

Selective halogenation of central and end-units of nonfullerene acceptors enables enhanced molecular packing and photovoltaic performance

Meiling Xie,‡[ab] Yanan Shi,‡[ab] Lingyun Zhu,*[a] Jianqi Zhang,[a] Qian Cheng,[ab] Hao Zhang,[ab] Yangjun Yan,[a] Mingquan Zhu,[ab] Huiqiong Zhou,[ab] Kun Lu,*[ab] and Zhixiang Wei[ab]

[a] CAS Key Laboratory of Nanosystem and Hierarchical Fabrication, CAS Center for Excellence in Nanoscience, National Center for Nanoscience and Technology, Beijing 100190, China

[b] University of Chinese Academy of Sciences, Beijing 100049, China

‡ These authors contributed equally.

* E-mail: zhuly@nanoctr.cn, lvk@nanoctr.cn

1. Experimental Section

1.1 Materials

Unless stated otherwise, all the reagents were obtained from commercial suppliers and used without further purification. PM6 and PNDIT-F3N were purchased from Solarmer Materials Inc., and 2PACz were purchased from TCI. The pre-patterned ITO glass and the mask used for depositing were purchased from Advanced Election Technology Co., Ltd. Compound 1, compound 5, and compound 6 were purchased from Hyper Chemical Company. Compound 2-1, compound 2-2, and compound 2-3 and were purchased from Bide Pharmatech Ltd.

1.2 Synthesis

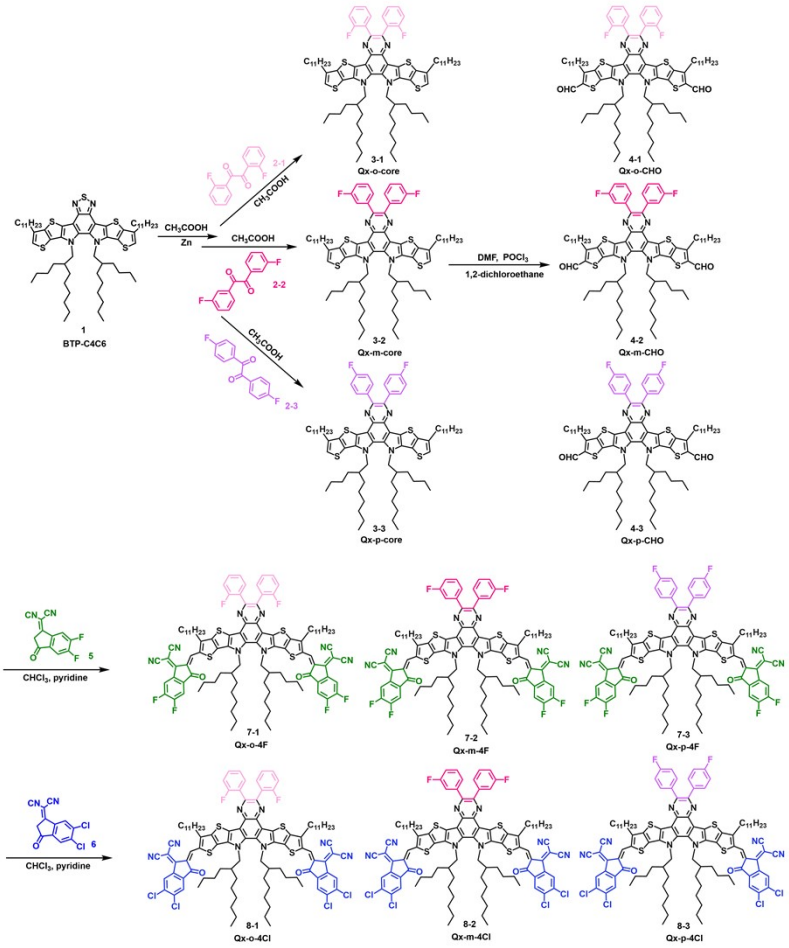

Scheme S1 Synthetic routes of these Qx-based acceptors.

After the reduction of compound 1 (BTP-C4C6), compound 3-1 (Qx-o-core), compound 3-2 (Qx-m-core), and compound 3-3 (Qx-p-core) were obtained by Schiff base reaction with compound 2-1, compound 2-2, or compound 2-3, respectively.[1, 2] Compound 3-1 (Qx-o-core),

compound 3-2 (Qx-m-core), and compound 3-3 (Qx-p-core) with the newly prepared Vilsmeier reagent (DMF and POCl3) in 1,2-dichloroethane produced compound 4-1 (Qx-o-CHO), compound 4-2 (Qx-m-CHO), and compound 4-3 (Qx-p-CHO), respectively.[3] The target molecules were synthesized by Knoevenagel reaction between compound 4-1, compound 4-2, and compound 4-3 and electron-withdrawing end-groups (compound 5 or compound 6) in a high yield over 80%.

Detailed synthetic process

Compound 3-1 (Qx-o-core): To a solution of compound 1(1.00 g, 0.923 mmol) in acetic acid (50 mL) was added zinc powder (2.40 g, 36.91 mmol) in one portion. Then the mixture solution was heated to 90°C for 5 h. After the solution was cooled at room temperature, the solid was removed by filtration. Transfer the filtrate to a three-tip flask containing compound 2-1 (909 mg, 3.69 mmol), then the mixture solution was heated to 110°C for 20 h. After cooling to room temperature, washed with saturated salt water and methylene chloride. The solvent was removed under reduced pressure. The crude product was subsequently purified by column chromatography on silica gel to afford compound 3-1 as yellow oily solid (421 mg, 36% yield). ^{1}H NMR (400 MHz, $CDCl_3$) δ 7.93 (d, J = 6.2 Hz, 2H), 7.47 – 7.38 (m, 2H), 7.35 (t, J = 7.1 Hz, 2H), 7.05 – 6.97 (m, 4H), 4.71 (d, J = 7.7 Hz, 4H), 2.85 (t, J = 7.6 Hz, 4H), 2.25 – 2.13 (m, 2H), 1.92 – 1.83 (m, 4H), 1.38 (d, J = 65.0 Hz, 34H), 1.13 – 0.94 (m, 20H), 0.90 (t, J = 6.6 Hz, 16H), 0.72 – 0.65 (m, 12H).

Compound 3-2 (Qx-m-core): was synthesized by similar procedure as compound 3-1 between compound 1 and compound 2-2. The final product were obtained as yellow solid (407 mg, 34.8% yield). ^{1}H NMR (400 MHz, $CDCl_3$) δ 7.82 (dd, *J* = 8.4, 5.5 Hz, 4H), 7.17 (t, *J* = 8.6 Hz, 4H), 7.05 (s, 2H), 4.70 (d, *J* = 7.5 Hz, 4H), 2.89 (t, *J* = 7.5 Hz, 4H), 2.18 (d, *J* = 5.5 Hz, 2H), 1.97 – 1.83 (m, 4H), 1.50 – 1.24 (m, 34H), 1.00 (dd, *J* = 12.4, 6.4 Hz, 20H), 0.91 (t, *J* = 6.5 Hz, 16H), 0.69 (dd, *J* = 7.2, 5.4 Hz, 12H).

Compound 3-3 (Qx-p-core): was synthesized by similar procedure as compound 3-1 between compound 1 and compound 2-3. The final product were obtained as yellow solid (444 mg, 38% yield). ^{1}H NMR (400 MHz, $CDCl_3$) δ 7.85 (s, 4H), 7.19 (t, *J* = 8.4 Hz, 4H), 7.07 (s, 2H), 4.74 (d, *J* = 5.5 Hz, 4H), 2.91 (t, *J* = 7.3 Hz, 4H), 2.24 (d, *J* = 6.3 Hz, 2H), 1.99 – 1.89 (m, 4H), 1.52 – 1.31 (m, 34H), 1.02 (dd, *J* = 12.9, 6.2 Hz, 20H), 0.93 (d, *J* = 7.0 Hz, 16H), 0.70 (dd, *J* = 13.8, 6.5 Hz, 12H).

Compound 4-1 (Qx-o-CHO): Compounds 3-1 (300 mg; 0.237 mmol) were dissolved into 1,2-dichloroethane (30 ml) in a three-neck flask. The solution was flushed with nitrogen in 0°C for 30 min. Then, add $POCl_3$ (0.40 mL) and DMF (0.40 mL) to the solution, then let the solution temperature return to room temperature for 1h. Next, the solution was reacted at 85 °C for 16 h under nitrogen protection. After that the mixture was poured into ice water (50 mL), neutralized with aqueous AcONa. Washed with saturated salt water and dichloromethane. The solvent was removed under reduced pressure. The crude product was subsequently purified by column chromatography on silica gel to afford compound 4-1 as orange solid (263 mg, 84% yield). ^{1}H NMR (400 MHz, $CDCl_3$) δ 10.19 (s, 2H), 7.91 (t, *J* = 6.9 Hz, 2H), 7.48 – 7.31 (m, 4H), 7.04 (t, *J* = 9.0 Hz, 2H), 4.76 (d, *J* = 6.4 Hz, 4H), 3.24 (t, *J* = 7.2 Hz, 4H), 2.19 (s, 2H), 1.97 – 1.90 (m, 4H), 1.29 (s, 34H), 1.04 – 0.95 (m, 16H), 0.91 – 0.88 (m, 20H), 0.71 (dd, *J* = 13.4, 6.6 Hz, 12H).

Compound 4-2 (Qx-m-CHO): was synthesized by similar procedure as compound 4-1 with compound 3-2. The final product were obtained as orange solid (251 mg, 80% yield). ^{1}H NMR (400 MHz, $CDCl_3$) δ 10.18 (s, 2H), 7.61 (d, *J* = 9.7 Hz, 2H), 7.48 (d, *J* = 7.7 Hz, 2H), 7.41 (dt, *J* = 13.6, 6.9 Hz, 2H), 7.17 (td, *J* = 8.4, 2.1 Hz, 2H), 4.72 (d, *J* = 7.7 Hz, 4H), 3.26 (t, *J* = 7.6 Hz, 4H), 2.14 (s, 2H), 2.00 – 1.91 (m, 4H), 1.31 (d, *J* = 25.8 Hz, 34H), 1.16 – 1.02 (m, 12H), 0.92 (s, 24H), 0.71 – 0.62 (m, 12H).

Compound 4-3 (Qx-p-CHO): was synthesized by similar procedure as compound 4-1 with compound 3-3. The final product were obtained as orange solid (276 mg, 88% yield). ^{1}H NMR (400 MHz, $CDCl_3$) δ 10.19 (s, 2H), 7.81 (dd, J = 8.3, 5.5 Hz, 4H), 7.18 (t, J = 8.6 Hz, 4H), 4.74 (d, J = 7.2 Hz, 4H), 3.26 (t, J = 7.4 Hz, 4H), 2.17 (s, 2H), 2.01 – 1.91 (m, 4H), 1.52 – 1.27 (m, 34H), 1.09 – 0.95 (m, 16H), 0.94 – 0.80 (m, 20H), 0.72 – 0.65 (m, 12H).

Compound 7-1 (Qx-o-4F): Compound 4-1 (200 mg, 0.151 mmol) and compound 5 (278 mg, 1.20 mmol) were dissolved into dry chloroform (60 mL) in a three-neck flask. The solution was flushed with nitrogen for 20 min. After 0.8 mL pyridine were added, the mixture was stirred at 65°C overnight. After cooling to room temperature, the reaction mixture was poured into water and extracted several times with chloroform. Then the solvent was removed under reduced pressure, and the crude product was purified by column chromatography on silica gel to yield Qx-o-4F as black solid (211 mg, 80% yield). ^{1}H NMR (400 MHz, $CDCl_3$) δ 9.20 (s, 2H), 8.61 (dd, J = 9.9, 6.5 Hz, 2H), 7.87 (t, J = 6.9 Hz, 2H), 7.73 (t, J = 7.5 Hz, 2H), 7.46 (dd, J = 12.8, 6.0 Hz, 2H), 7.37 (t, J = 7.4 Hz, 2H), 7.09 – 7.01 (m, 2H), 4.92

– 4.77 (m, 4H), 3.27 (t, J = 7.5 Hz, 4H), 2.27 – 2.19 (m, 2H), 1.95 – 1.82 (m, 4H), 1.60 – 1.48 (m, 12H), 1.32 (dd, J = 39.1, 6.8 Hz, 30H), 1.20 – 0.96 (m, 20H), 0.88 (dd, J = 12.2, 5.7 Hz, 8H), 0.71 (ddd, J = 22.1, 14.4, 7.3 Hz, 12H). ^{13}C NMR (101 MHz, $CDCl_3$) δ 186.27, 161.22, 158.74, 155.82, 155.68, 153.19, 153.05, 148.09, 136.83, 135.15, 134.62, 133.59, 132.34, 131.14, 131.03, 127.66, 127.50, 124.44, 119.68, 115.98, 115.76, 115.18, 114.96, 112.59, 112.40, 55.79, 39.29, 32.05, 31.75, 31.60, 30.62, 30.53, 30.43, 29.89, 29.81, 29.75, 29.65, 29.63, 29.60, 29.57, 29.48, 28.20, 28.07, 25.59, 25.45, 23.06, 23.03, 22.83, 22.63, 22.62, 14.25, 14.17, 14.16, 13.99, 13.97.

Compound 7-2 (Qx-m-4F): was synthesized by similar procedure as Qx-o-4F between compound 4-2 and compound 5. The final product were obtained as black solid (224 mg, 85% yield). ^{1}H NMR (400 MHz, $CDCl_3$) δ 9.21 (s, 2H), 8.61 (dd, *J* = 10.0, 6.5 Hz, 2H), 7.73 (t, *J* = 7.5 Hz, 2H), 7.59 (d, *J* = 9.4 Hz, 2H), 7.51 – 7.38 (m, 4H), 7.20 (dd, *J* = 8.9, 7.0 Hz, 2H), 4.87 (d, *J* = 18.1 Hz, 4H), 3.37 – 3.23 (m, 4H), 2.21 (s, 2H), 1.97 – 1.83 (m, 4H), 1.57 (s, 12H), 1.41 – 1.19 (m, 30H), 1.19 – 0.92 (m, 20H), 0.93 – 0.82 (m, 8H), 0.82 – 0.61 (m, 12H). ^{13}C NMR (101 MHz, $CDCl_3$) δ 186.27, 164.19, 161.75, 155.83, 155.68, 153.24, 153.05, 149.49, 141.40, 141.32, 136.81, 134.66, 133.66, 130.90, 130.10, 130.02, 126.23, 119.54, 117.32, 117.09, 116.23, 116.02, 115.16, 114.95, 112.59, 112.40, 55.80, 39.33, 32.05, 31.76, 31.61, 30.62, 30.54, 30.48, 29.86, 29.81, 29.76, 29.64, 29.61, 29.48, 28.19, 28.06, 25.63, 25.49, 23.06, 23.03, 22.83, 22.65, 22.63, 14.25, 14.19, 13.99, 13.96.

Compound 7-3 (Qx-p-4F): was synthesized by similar procedure as Qx-m-4F between compound 4-2 and compound 5. The final product were obtained as black solid (227 mg, 86% yield). ^{1}H NMR (400 MHz, $CDCl_3$) δ 9.19 (s, 2H), 8.59 (dd, J = 9.8, 6.5 Hz, 2H), 7.78 (dt, J = 11.2, 5.7 Hz, 4H), 7.55 (dd, J = 5.6, 3.3 Hz, 2H), 7.20 (t, J = 8.5 Hz, 4H), 4.82 (d, J = 23.3 Hz, 4H), 3.29 (t, J = 7.4 Hz, 4H), 2.19 (s, 2H), 1.87 (d, *J* = 7.4 Hz, 4H), 1.54 (s, 10H), 1.25 (s, 30H), 1.12 – 0.90 (m, 20H), 0.86 (dd, *J* = 12.6, 6.1 Hz, 8H), 0.68 (ddd, *J* = 23.3, 12.6, 7.2 Hz, 12H). ^{13}C NMR (101 MHz, $CDCl_3$) δ 186.28, 164.68, 162.19, 158.97, 155.81, 155.67, 153.23, 153.10, 149.81, 136.81, 135.43, 135.40, 134.62, 133.53, 132.28, 132.20, 130.86, 130.84, 119.61, 115.87, 115.65, 115.18, 114.96, 114.77, 112.56, 112.39, 68.49, 55.77, 39.33, 32.05, 31.76, 31.60, 30.54, 29.88, 29.84, 29.77, 29.66, 29.63, 29.61, 29.48, 28.19, 28.07, 25.64, 25.50, 23.06, 23.03, 22.82, 22.65, 22.63, 14.25, 14.19, 13.99, 13.96.

Compound 8-1 (Qx-o-4Cl): was synthesized by similar procedure as Qx-m-4F between compound 4-1 and compound 6. The final product were obtained as black solid (224 mg,

82% yield). ^{1}H NMR (400 MHz, $CDCl_3$) δ 9.22 (s, 2H), 8.83 (s, 2H), 7.99 (s, 2H), 7.86 (t, *J* = 6.8 Hz, 2H), 7.47 (dd, *J* = 13.0, 5.9 Hz, 2H), 7.37 (t, *J* = 7.5 Hz, 2H), 7.08 – 7.02 (m, 2H), 4.85 (d, *J* = 7.4 Hz, 4H), 3.27 (t, *J* = 7.7 Hz, 4H), 2.23 (dd, *J* = 11.0, 6.6 Hz, 2H), 1.94 – 1.84 (m, 4H), 1.59 – 1.51 (m, 12H), 1.28 (d, *J* = 7.8 Hz, 30H), 1.17 – 0.97 (m, 20H), 0.88 (t, *J* = 6.8 Hz, 8H), 0.72 (ddd, *J* = 23.6, 13.0, 7.3 Hz, 12H).

Compound 8-2 (Qx-m-4Cl): was synthesized by similar procedure as Qx-m-4F between compound 4-2 and compound 6. The final product were obtained as black solid (213 mg, 78% yield). ^{1}H NMR (400 MHz, $CDCl_3$) δ 9.20 (s, 2H), 8.81 (s, 2H), 7.97 (s, 2H), 7.56 (d, *J* = 9.5 Hz, 2H), 7.43 (dt, *J* = 13.5, 7.6 Hz, 4H), 7.17 (t, *J* = 8.1 Hz, 2H), 4.82 (d, *J* = 7.6 Hz, 4H), 3.28 (t, *J* = 7.6 Hz, 4H), 2.19 (s, 2H), 1.96 – 1.81 (m, 4H), 1.52 (d, *J* = 20.5 Hz, 12H), 1.41 – 1.19 (m, 30H), 1.16 – 0.90 (m, 20H), 0.90 – 0.76 (m, 8H), 0.68 (ddd, *J* = 24.2, 12.8, 7.2 Hz, 12H).

Compound 8-3 (Qx-p-4Cl): was synthesized by similar procedure as Qx-m-4F between compound 4-2 and compound 6. The final product were obtained as black solid (219 mg, 80% yield). ^{1}H NMR (400 MHz, $CDCl_3$) δ 9.19 (s, 2H), 8.81 (s, 2H), 7.96 (s, 2H), 7.76 (dd, J = 8.6, 5.4 Hz, 4H), 7.17 (t, J = 8.6 Hz, 4H), 4.81 (d, J = 7.9 Hz, 4H), 3.27 (t, J = 7.6 Hz, 4H), 2.20 (d, J = 8.8 Hz, 2H), 1.93 – 1.81 (m, 4H), 1.54 (s, 12H), 1.34 – 1.14 (m, 30H), 1.12 – 0.90 (m, 20H), 0.86 (dd, J = 12.6, 6.1 Hz, 8H), 0.68 (ddd, J = 23.3, 12.6, 7.2 Hz, 12H). ^{13}C NMR (101 MHz, $CDCl_3$) δ 186.30, 164.68, 162.20, 158.75, 149.93, 139.48, 139.16, 138.86, 136.18, 135.41, 135.38, 134.61, 133.60, 132.30, 132.22, 131.13, 126.97, 124.97, 119.66, 115.87, 115.66, 115.27, 114.80, 68.52, 55.79, 39.38, 32.05, 31.80, 31.56, 30.68, 30.61, 29.88, 29.84, 29.77, 29.69, 29.66, 29.64, 29.48, 28.25, 28.16, 25.79, 25.68, 23.06, 23.03, 22.82, 22.67, 14.25, 14.22, 14.00, 13.98.

1.3 Methods and measurements

Molecular properties

^{1}H NMR was obtained on a Bruker Avance Ⅲ 400 NMR Spectrometer (operating at 400 MHz, using $CDCl_3$ as solvent using tetramethylsilane as internal standard). The UV-vis absorption were measured by Shimadzu UV-3600 spectrophotometer. The electrochemical cyclic voltammetry (CV) was conducted an electrochemical workstation (VMP3 Biologic, France) with a Pt disk coated with blend film, a Pt plate, and an Ag^+/Ag electrode acting as the working, counter, and reference electrodes, respectively, in a 0.1 mol/L tetrabutylammonium phosphorus hexafluoride (Bu_4NPF_6) acetonitrile solution. The

experiments were calibrated with the standard ferrocene/ferrocenium (Fe) redox system and assumption that the energy level of Fe is 4.8 eV below vacuum.

Single-crystal growth

Single crystals of Qx-o-F and Qx-m-4F were grown by the liquid diffusion method at room temperature. An appropriate amount of methanol is transferred to a concentrated chloroform solution, which will form crystals over time. Single crystal diffraction was collected at low temperatures protected by liquid nitrogen in accordance with standard procedures for reducing X-ray radiation damage through the use of the single-crystal X-ray diffractometer (model is XtaLAB PRO 007HF(Mo), manufactured by Rigaku). The X-ray crystallographic coordinates for structures reported of Qx-o-F and Qx-m-4F have been deposited at the Cambridge Crystallographic Data Centre (CCDC), under deposition numbers 2253303 and 2253302.

Device fabrication and characterization

The devices were fabricated with a conventional structure of ITO/PEDOT:PSS (or 2PACz)/active layer/PNDIT-F3N/Ag. The ITO-coated glass were cleaned under sonication for 30 minutes with detergent, deionized water, ethanol and isopropyl alcohol sequentially. After drying, the substrates were treated with UV-ozone for 15 minutes. For PEDOT:PSS-based devices, PEDOT:PSS (Heraeus, CLEVIOS P VP AI4083, filtered at 0.45 μm) was deposited by spin-coating under 3500 rpm for 30 s onto ITO substrate and then thermal annealed for 15 minutes at 150 ℃. For 2PACz-based devices, 2PACz (0.3mg mL^{-1} in ethanol) was spin-coated onto ITO for 30 seconds and then annealed at 100 ℃ for 10 minutes. Then and acceptor materials were dissolved in chloroform (CF) solvent with a total concentration of 14 mg/ml (donor: acceptor = 1:1.2 w/w) and then stirred at 50 ℃ for 60 minutes. 1-Chloronaphthalene (CN) was then added into the solvent at the volume fraction of 0.6% or 0.8% (0.6% for PM6:Qx-m-4F, PM6:Qx-p-4F, and PM6:Qx-p-4Cl; 0.8% for PM6:Qx-o-4F). The blend solution was spin-coated at 2500-3500 rpm for 30 s to form a thin film on the substrate. After thermal annealing at 90-110 ℃ (90 ℃ for PM6:Qx-o-4F; 100 ℃ for PM6:Qx-m-4F; 110 ℃ for PM6:Qx-p-4F and PM6:Qx-p-4Cl) for 10 min, PNDIT-F3N (0.5 mg mL^{-1}, in methanol with 0.5% v/v acetic acid) was spin-coated onto the top of the active layer as an

electron transport layer at 3000 rpm for 30 s. Finally, Finally, a layer of Ag with a thickness of 150 nm was vacuum-deposited under 1×10^{-4} Pa. Except for the fabrication of PEDOT:PSS layer, the other processes were all carried out in a nitrogen-filled glovebox.

The active area of the device was approximately 4 mm^2. The whole photovoltaic performance characterization was processed in a nitrogen-filled glovebox with a 2.56 mm^2 mask. The *J-V* measurements were conducted via the solar simulator (SS-F5-3A, Enlitech) under AM 1.5 G illumination, whose light intensity was calibrated by the standard silicon solar cell (SRC-2020, Enlitech) with a KG2 filter. *J–V* curves were recorded by Keithley 2400 source-measure unit. The EQE measurements were performed through a solar cell spectral response measurement system (QER3011, Enlitech), and the intensity was calibrated with a standard single crystal Si photovoltaic cell.

Transient photocurrent (TPC) and transient photovoltage (TPV) were measured by applying a 488 nm solid-state laser (Coherent OBIS CORE 488LS) with a pulse width of ~30 ns. The current traces were recorded by a mixed domain oscilloscope (Tektronix MDO3032) through converting the registered voltage drop across a 2 Ω resistor load connected in series to the solar cell. The photovoltage traces were registered by the oscilloscope with an external 10 MΩ resistor in series.

Charge carrier mobility characterization

Hole and electron mobilities were measured by the space-charge limited current (SCLC) method with hole-only devices and electron-only devices. The hole-only devices adopted ITO/PEDOT:PSS/active layer/MoO_x/Ag structure, while electron-only devices adopting ITO/ZnO/active layer/PNDIT-F3N/Ag structure. The active layers for these two devices were spincoated under the same condition as that of solar cells. *J–V* curves in the range of 0 to 5 V were gained by Keithley 2400 source-measure unit in the dark condition.

The mobilities were obtained by fitting *J-V* curves with the equation:

$$J = \frac{9\varepsilon_r\varepsilon_0\mu V^2}{8L^3} exp\left(0.89\gamma\sqrt{\frac{V}{L}}\right) \qquad (1)$$

where J is the current density, L is the thickness of the active layer, μ is the zero-field mobility, ε_0 is the vacuum dielectric constant, ε_r is the relative dielectric constant of the transport medium, and γ is a constant. V (= V_{app} - V_{bi}) is the internal voltage, where V_{app} is the applied voltage and V_{bi} is the built-in voltage.

In this case, the charge mobilities were estimated by the equation:

$$\ln(\frac{JL^3}{V^2}) = 0.89\gamma\sqrt{\frac{V}{L}} + \ln(\frac{9}{8}\varepsilon_r\varepsilon_0\mu_0) \qquad (2)$$

Morphology and crystallization characterization

Atomic force microscopy (AFM) images of the blend films were obtained from the devices directly on a VEECO Dimension 3100 atomic force microscope working under ScanAsys mode. Transmission electron microscopy (TEM) characterization was performed by Tecnai G2 F20 U-TWIN TEM instrument.Grazing incidence wide-angle X-ray scattering (GIWAXS) characterizations were conducted at XEUSS SAXS/WAXS equipment.

Energy loss analysis

Fourier-transform photocurrent spectroscopy external quantum efficiency (FTPS-EQE) measurements were carried out by an integrated system (PECT600, Enlitech). The electroluminescence external quantum efficiency (EQE_{EL}) was obtained by applying an external voltage/current source through the integrated device (REPS, Enlitech).

Based on Shockley-Queisser limit theory, the energy loss (E_{loss}) in OSCs originates from three parts[4] as follows:

$$\begin{aligned} E_{loss} &= E_g^{PV} - qV_{OC} \\ &= \left(E_g^{PV} - qV_{OC}^{SQ}\right) + \left(qV_{OC}^{SQ} - qV_{OC}^{rad}\right) + \left(qV_{OC}^{rad} - qV_{OC}\right) \\ &= \left(E_g^{PV} - qV_{OC}^{SQ}\right) + q\Delta V_{OC}^{rad,belowgap} + q\Delta V_{OC}^{non\text{-}rad} \\ &= \Delta E_1 + \Delta E_2 + \Delta E_3 \end{aligned} \qquad (3)$$

where q is the elementary charge; V_{oc}^{SQ} is the maximum voltage by the *S-Q* limit; V_{oc}^{rad} is the open-circuit voltage when there is only radiative recombination in the device; $\Delta V_{oc}^{rad,\,belowgap}$ is the voltage loss of radiative recombination below the bandgap; $\Delta V_{oc}^{non\text{-}rad}$ is the voltage loss due to non-radiative recombination.

The photovoltaic bandgap energy (E_g^{PV}) obtained from the derivative of the EQE spectrum was used to determined bandgap.[5]

$$E_{\mathrm{g}}^{\mathrm{PV}}=\frac{\int_{\mathrm{a}}^{b} E_{\mathrm{g}}\mathrm{P}(E_{\mathrm{g}})\mathrm{d}E_{\mathrm{g}}}{\int_{\mathrm{a}}^{b}\mathrm{P}(E_{\mathrm{g}})\mathrm{d}E_{\mathrm{g}}} \qquad (4)$$

where P(E) = dEQE/dE, and the integral boundaries a and b are chosen as the P(a) = P(b) = 0.5max[P(Eg)].

The V_{oc}^{SQ} can be calculated by the equation:

$$V_{oc}^{SQ}=\frac{kT}{q}\ln\left(\frac{J_{sc}}{J_0^{SQ}}+1\right)=\frac{kT}{q}\ln\left(\frac{q\cdot\int_0^{\infty}EQE_{PV}(E)\phi_{AM1.5G}(E)dE}{q\cdot\int_{E_g}^{\infty}\phi_{BB}(E)dE}+1\right) \qquad (5)$$

Likewise, the V_{oc}^{rad} can be calculated as follow:

$$V_{oc}^{rad}=\frac{kT}{q}\ln\left(\frac{J_{sc}}{J_0^{rad}}+1\right)=\frac{kT}{q}\ln\left(\frac{q\cdot\int_0^{\infty}EQE_{PV}(E)\phi_{AM1.5G}(E)dE}{q\cdot\int_0^{\infty}EQE_{PV}(E)\phi_{BB}(E)dE}+1\right) \qquad (6)$$

where ϕ_{BB}(E) is the black body spectrum, given by:

$$\phi_{BB}(E)=\frac{2\pi E^2}{h^3c^2}\frac{1}{\left[\exp\left(\frac{E}{kT}\right)-1\right]}\approx\frac{2\pi E^2}{h^3c^2}\exp\left(\frac{-E}{kT}\right) \qquad (7)$$

where *k* is the Boltzmann constant, *T* is the temperature, *q* is the elementary charge, *h* is Planck's constant, *c* is the speed of light in vacuum, and the $\mathrm{EQE_{PV}}$ (*E*) is derived from FTPS-EQE measurements.

In addition, the nonradiative energy loss (ΔE_3) can be calculated by EQE_{EL} measurements:

$$\Delta E_3=-kT\ln\left(EQE_{EL}\right) \qquad (8)$$

2. Supplementary Figures

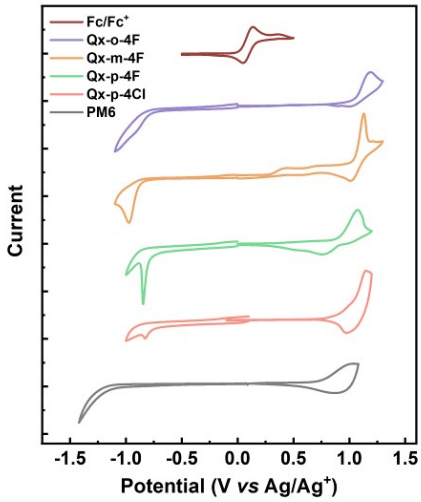

Fig. S1 Electrochemical cyclic voltammetry (CV) curves of these molecules measured in 0.1 mol L^{-1} Bu_4NPF_6 acetonitrile solutions.

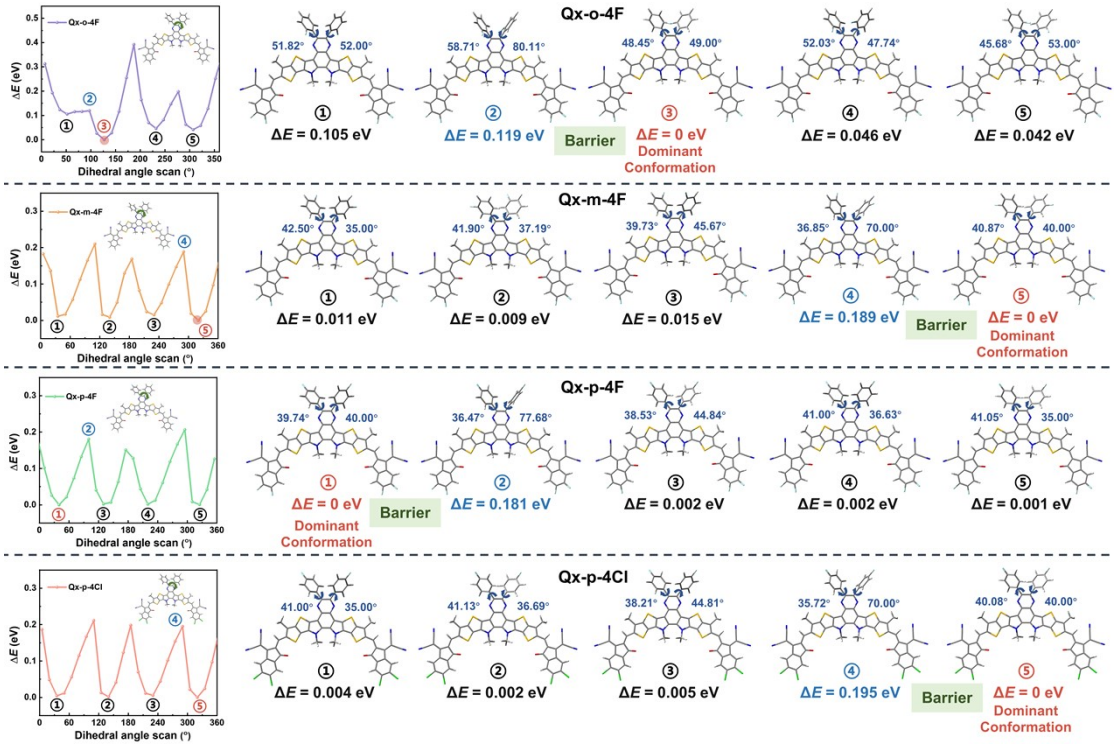

Fig. S2 Relaxed potential energy scan results and the relative energies (Δ*E*) of Qx-o-4F, Qx-m-4F, Qx-p-4F, and Qx-p-4Cl (the blue arrows indicated the fluorinated phenyl and Qx core torsions). For computational ease, all the alkyl chains of the four NFAs were replaced by methyl groups.

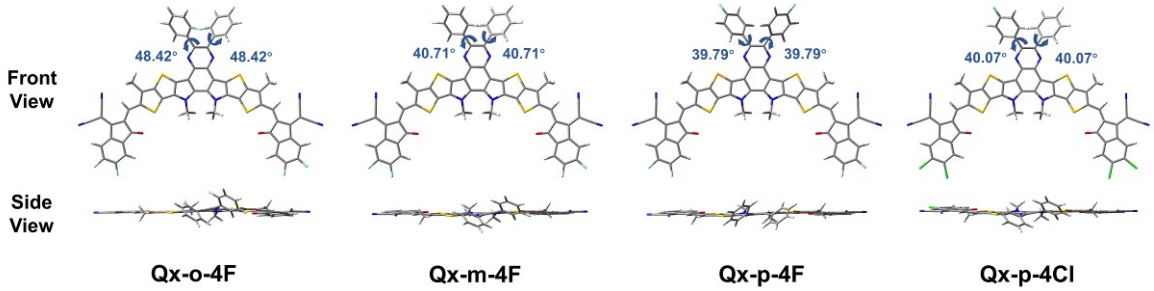

Fig. S3 Optimized molecular geometry for simplified molecules calculated from DFT at B3LYP/6-31G(d,p) level (the blue arrows indicated the fluorinated phenyl and Qx core torsions).

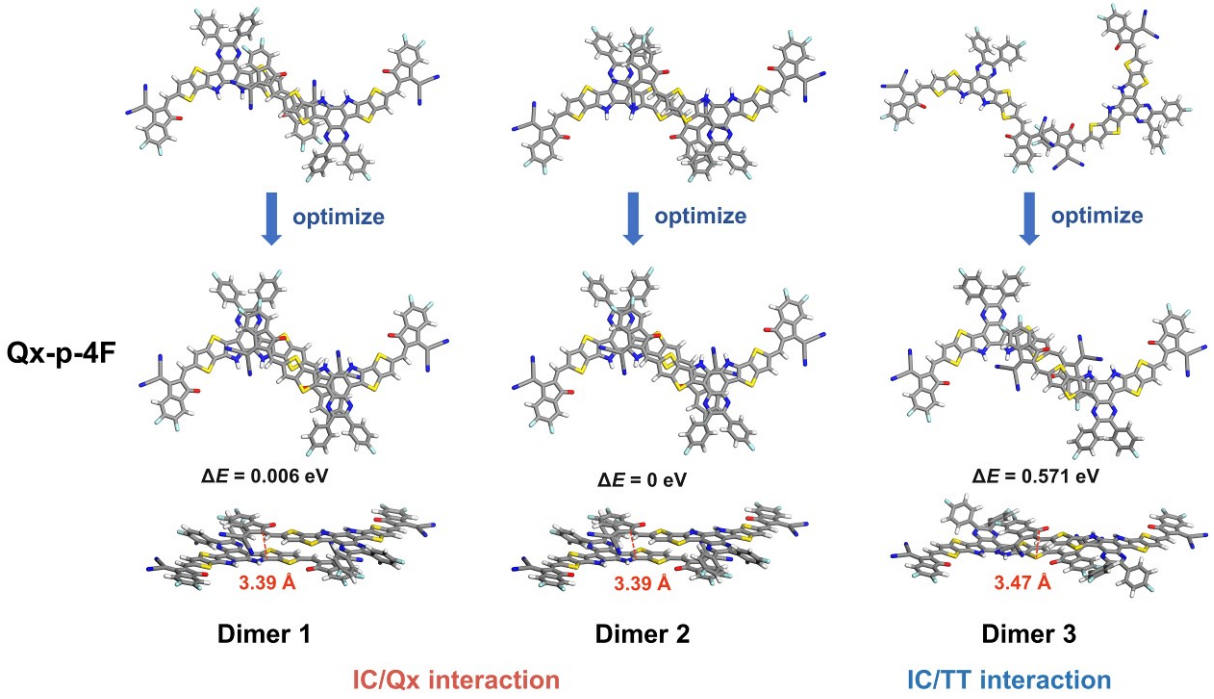

Fig. S4 The optimized geometries and the relative energies (Δ*E*) of three dimers for Qx-p-4F (DFT calculations were performed at the B3LYP-D/6-31G(d, p) level, including the dispersion correction).

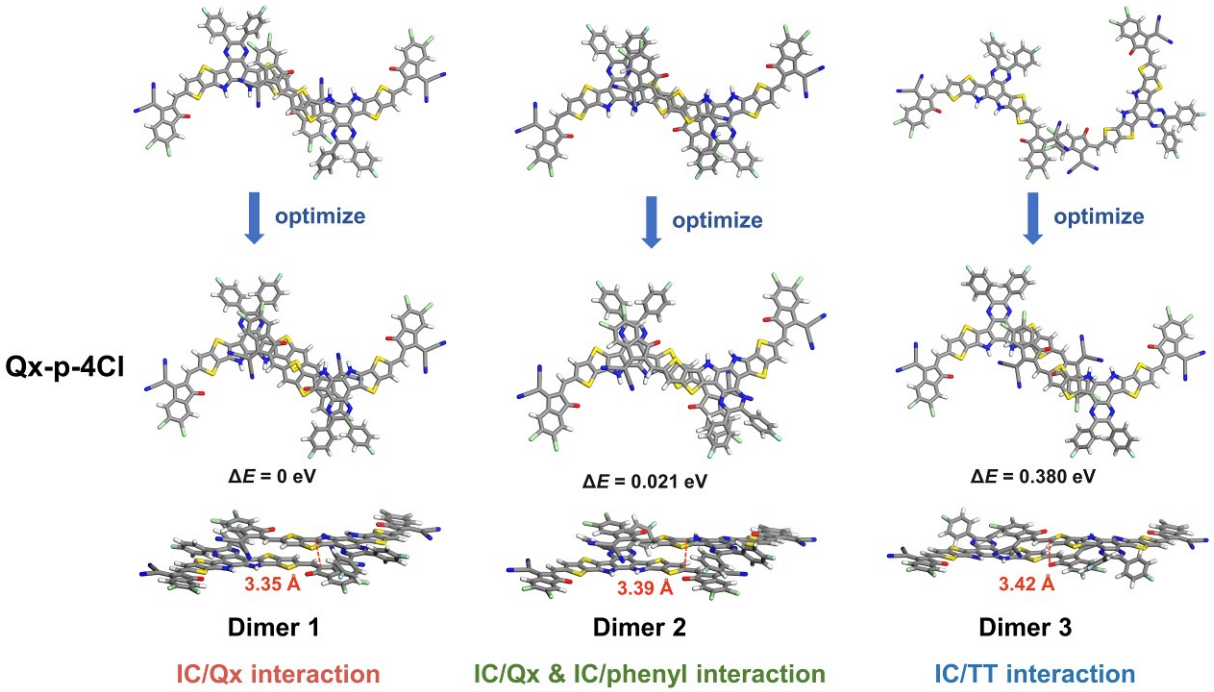

Fig. S5 The optimized geometries and the relative energies (Δ*E*) of three dimers for Qx-p-4Cl (DFT calculations were performed at the B3LYP-D/6-31G(d, p) level, including the dispersion correction).

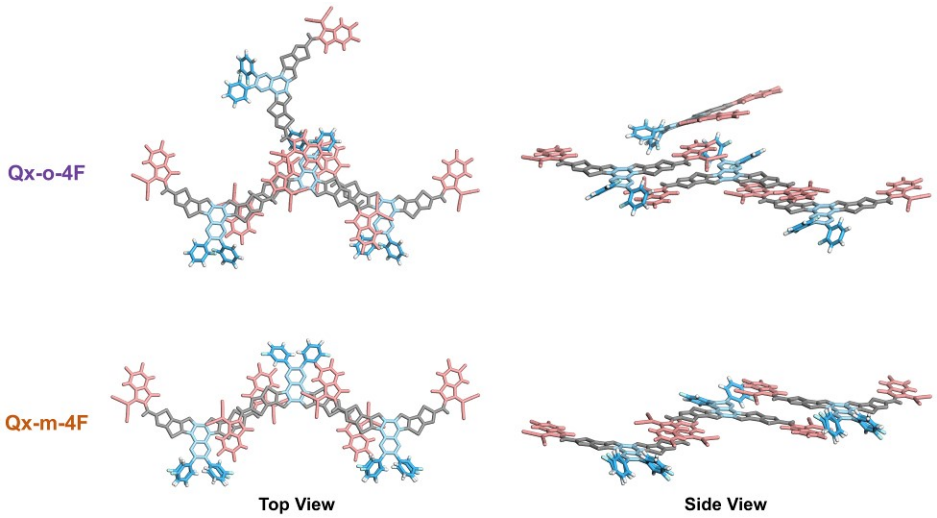

Fig. S6 The stacking diagrams of Qx-o-4F and Qx-m-4F formed by multiple dimers (the alkyl chains have been omitted for clarity).

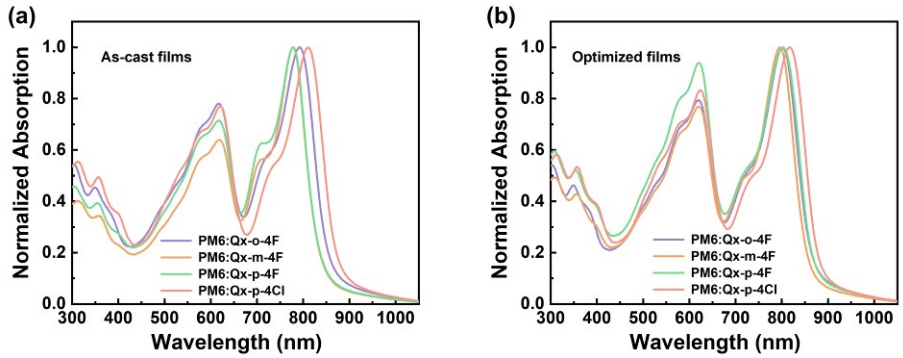

Fig. S7 Normalized UV-vis absorption spectra of the four blend films. a) before and b) after post-treatment.

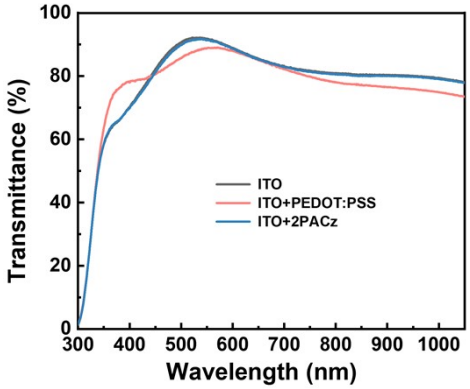

Fig. S8 Transmittance spectra of bare and HTL (PEDOT:PSS and 2PACz)-covered ITO glass.

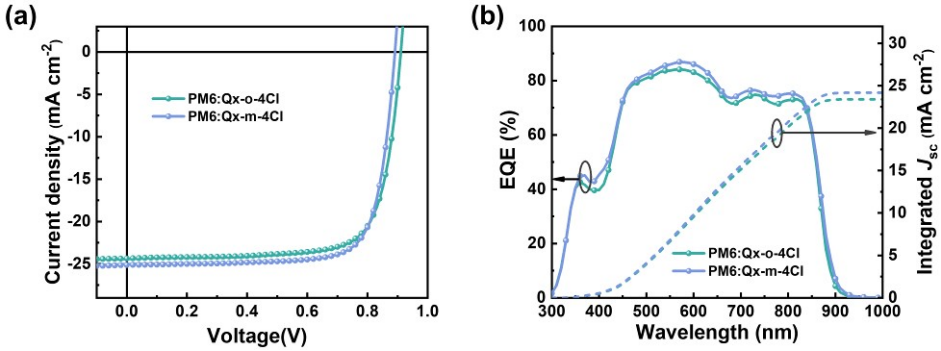

Fig. S9 (a) *J*–*V* curves and (b) EQE spectra of the optimal devices based on PM6:Qx-m-4Cl and PM6:Qx-o-4Cl.

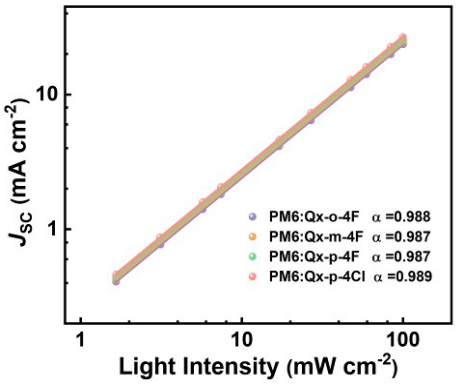

Fig. S10 Dependence of J_{SC} on the light intensity.

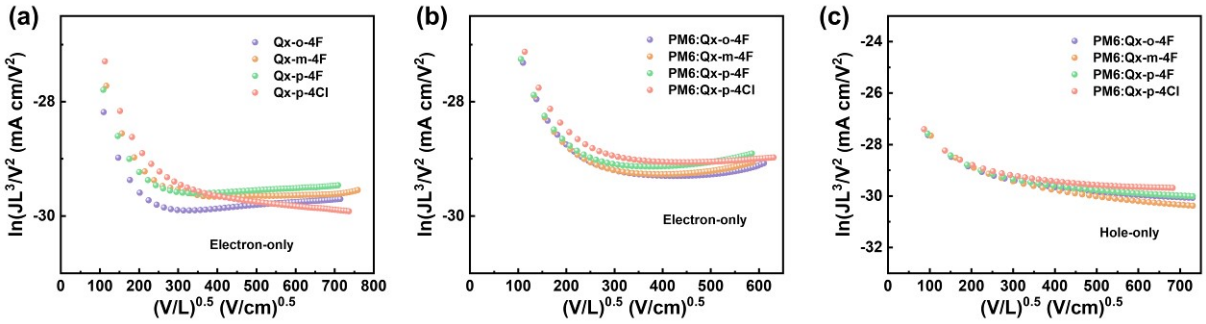

Fig. S11 The SCLC plots of a) electron-only devices for the neat acceptor films, b) electron-only devices and c) hole-only devices for the four blends.

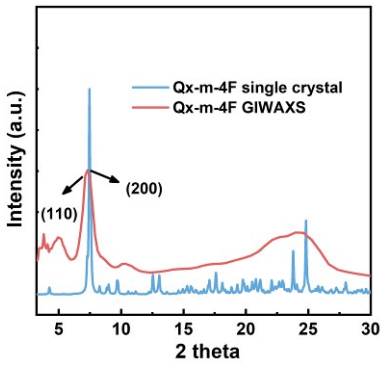

Fig. S12 The crystal patterns extracted from single crystal and GIWAXS data of Qx-m-4F.

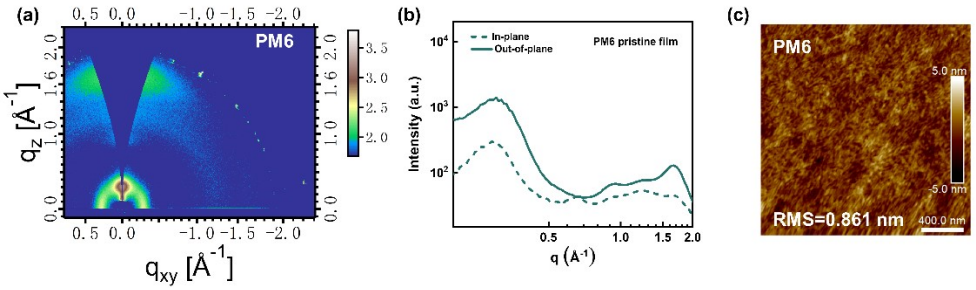

Fig. S13 a)2D GIWAXS pattern, b) the corresponding 1D line-cuts, and c) AFM image of PM6 pristine film.

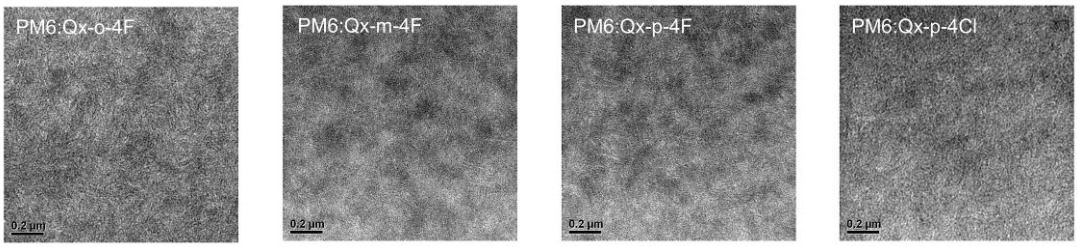

Fig. S14 TEM images of blend films.

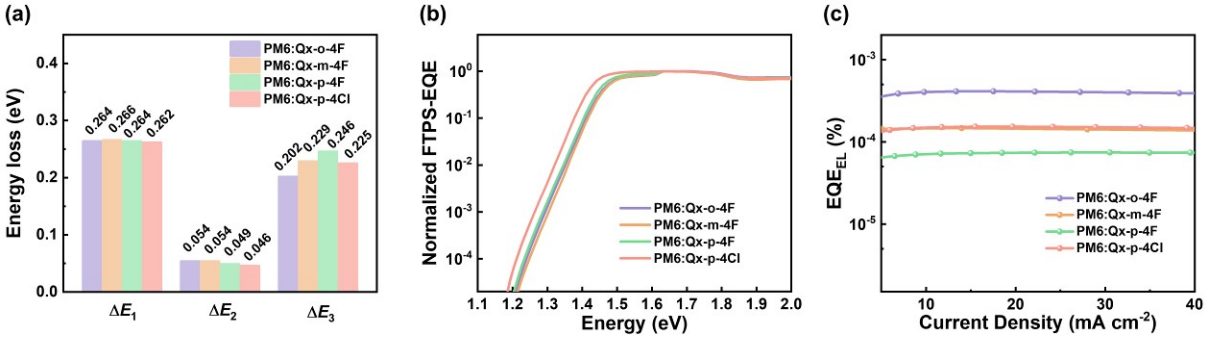

Fig. S15 a) Detailed energy losses for the four devices based on PM6:Qx-o-4F, PM6:Qx-m-4F, PM6:Qx-p-4F, and PM6:Qx-p-4Cl. b) FTPS-EQE spectra of the optimized devices. c) EQE_{EL} of the optimized devices measured at different injected currents.

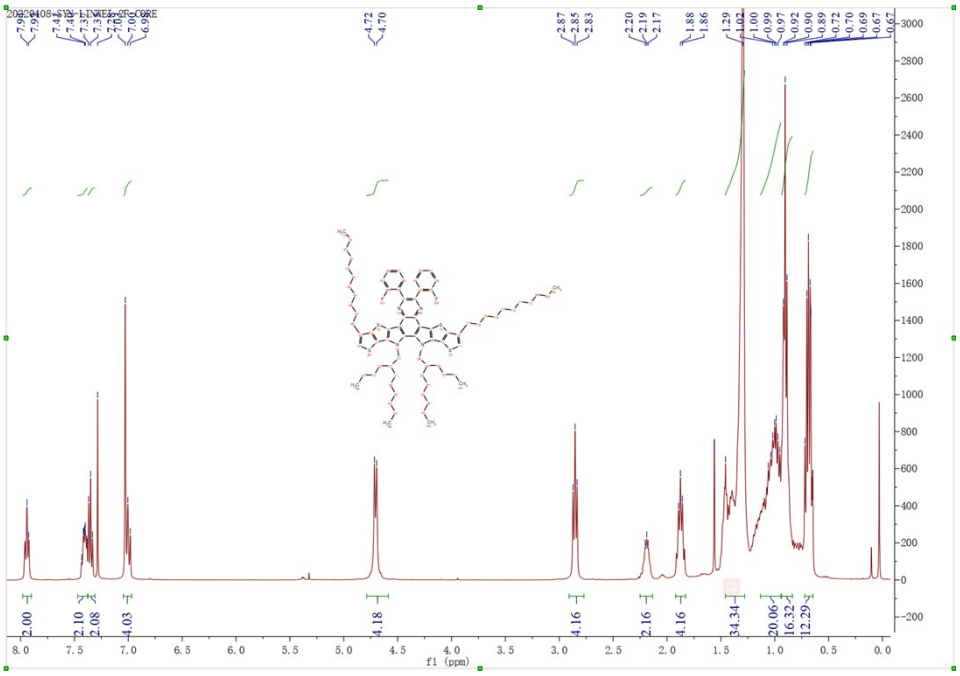

Fig. S16 ^{1}H NMR spectrum of Qx-o-core in $CDCl_3$.

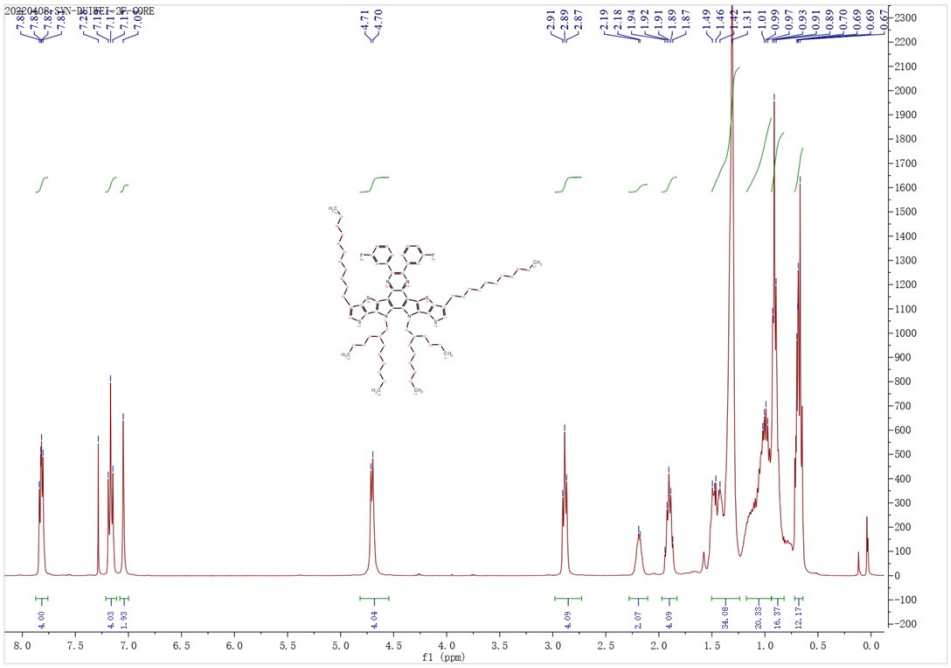

Fig. S17 ^{1}H NMR spectrum of Qx-m-core in $CDCl_3$.

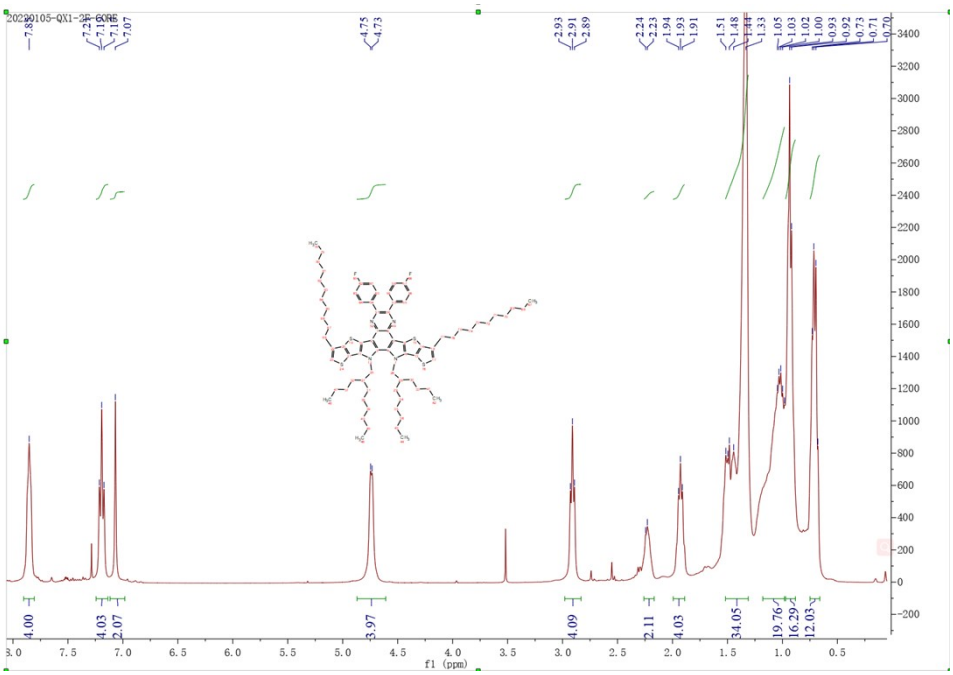

Fig. S18 ^{1}H NMR spectrum of Qx-p-core in $CDCl_3$.

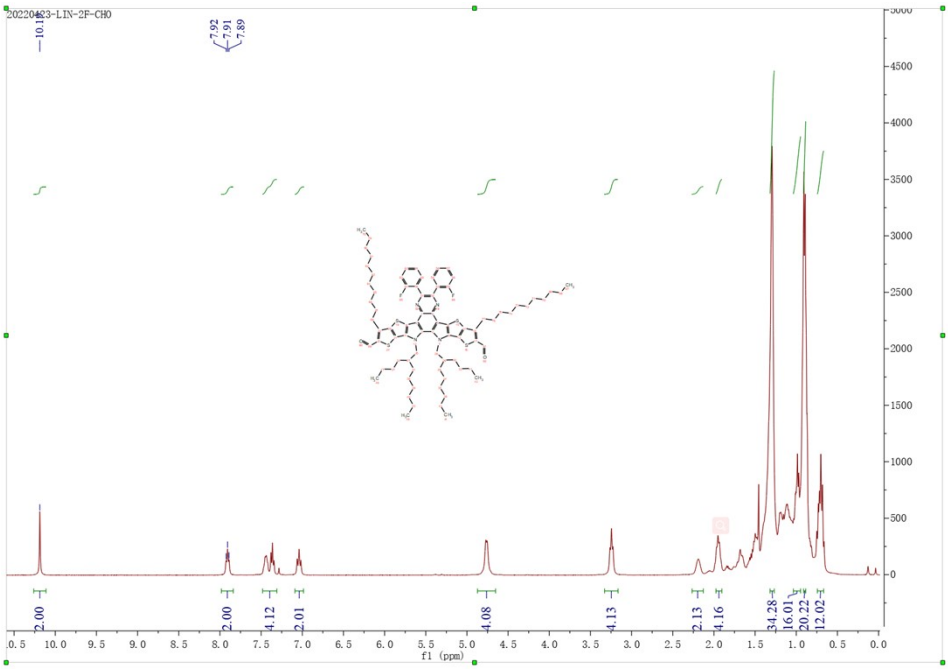

Fig. S19 ^{1}H NMR spectrum of Qx-o-CHO in $CDCl_3$.

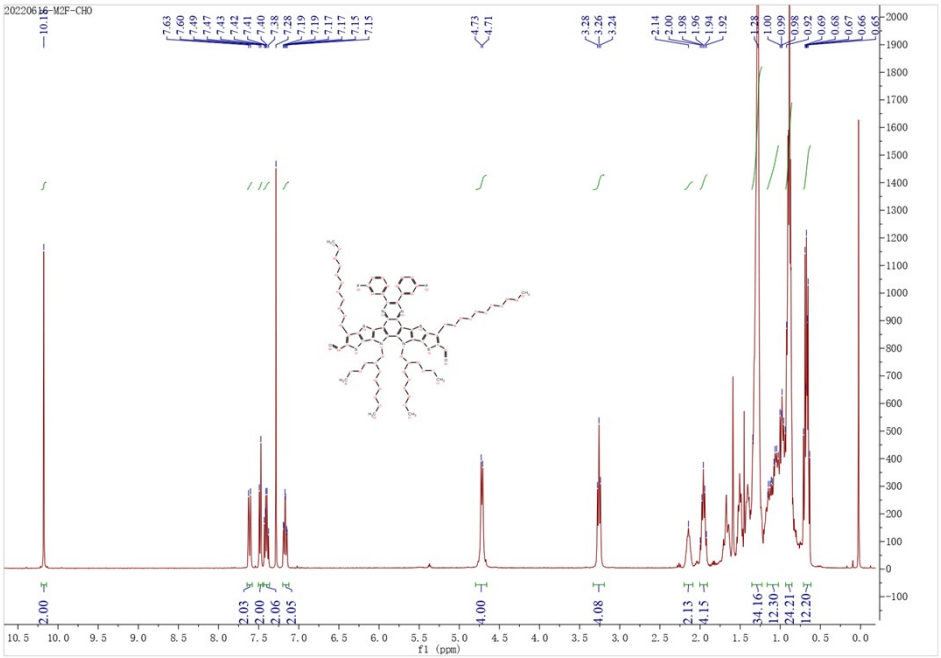

Fig. S20 ^{1}H NMR spectrum of Qx-m-CHO in $CDCl_3$.

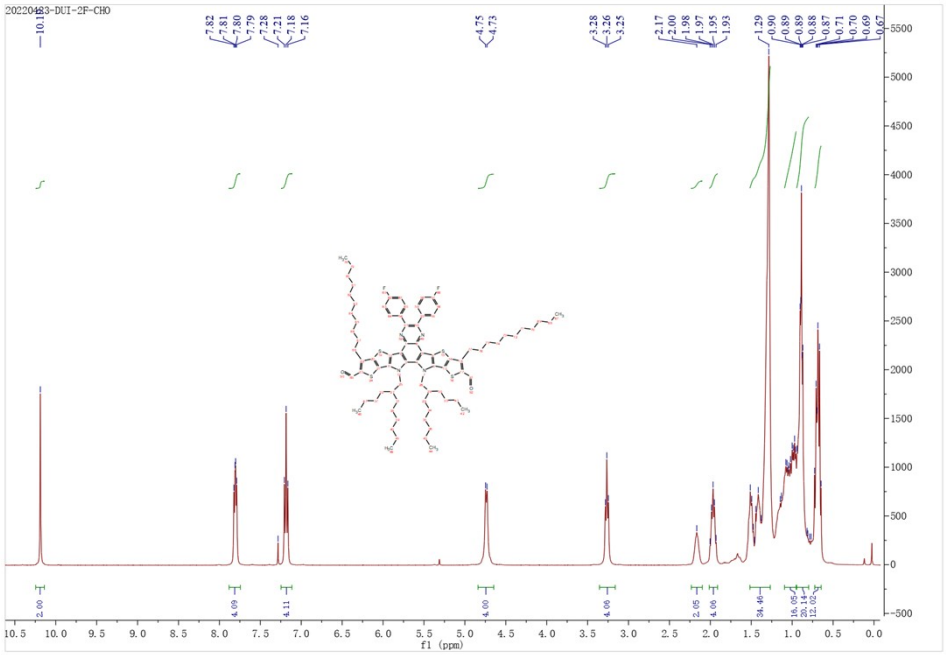

Fig. S21 ^{1}H NMR spectrum of Qx-p-CHO in $CDCl_3$.

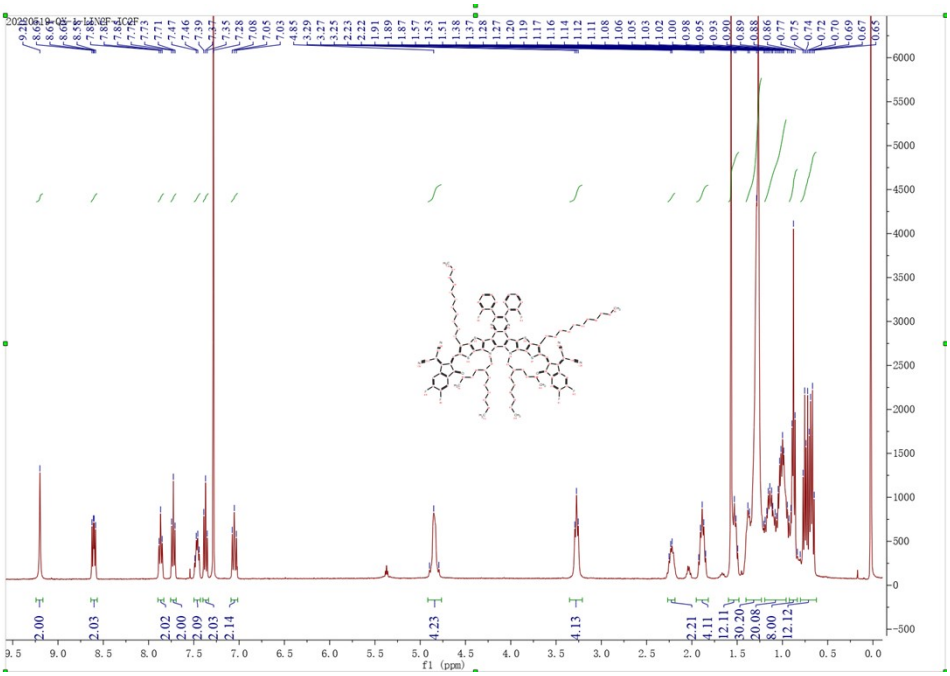

Fig. S22 ^{1}H NMR spectrum of Qx-o-4F in $CDCl_3$.

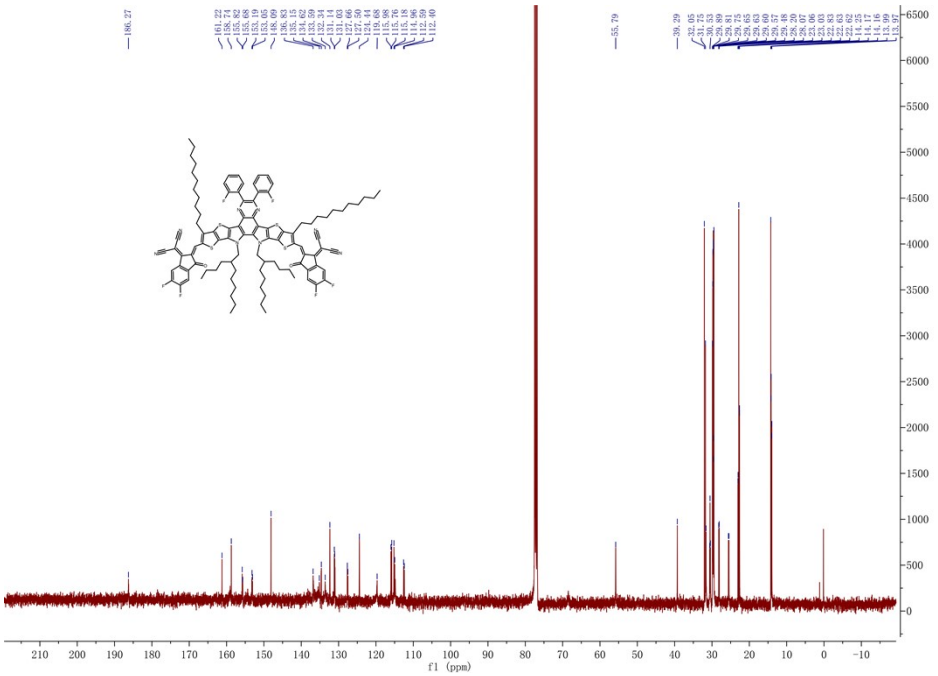

Fig. S23 ^{13}C NMR spectrum of Qx-o-4F in $CDCl_3$.

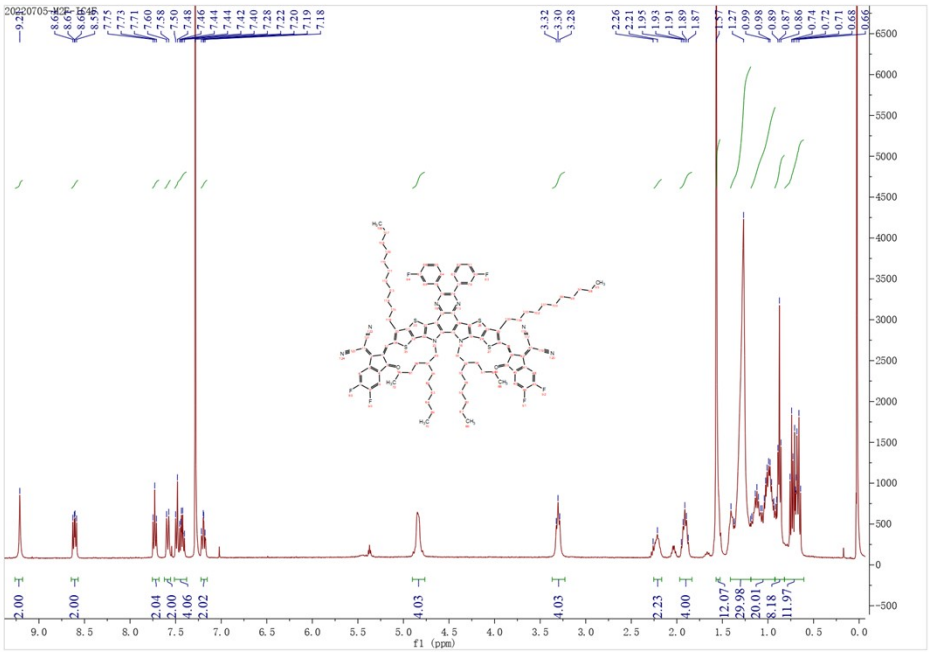

Fig. S24 ^{1}H NMR spectrum of Qx-m-4F in $CDCl_3$.

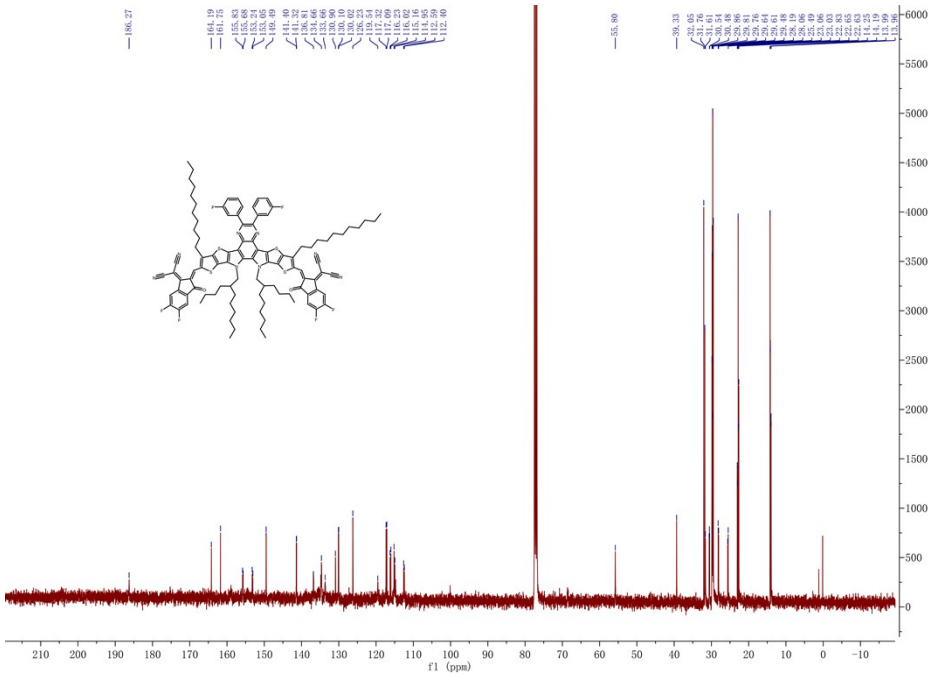

Fig. S25 ^{13}C NMR spectrum of Qx-m-4F in $CDCl_3$.

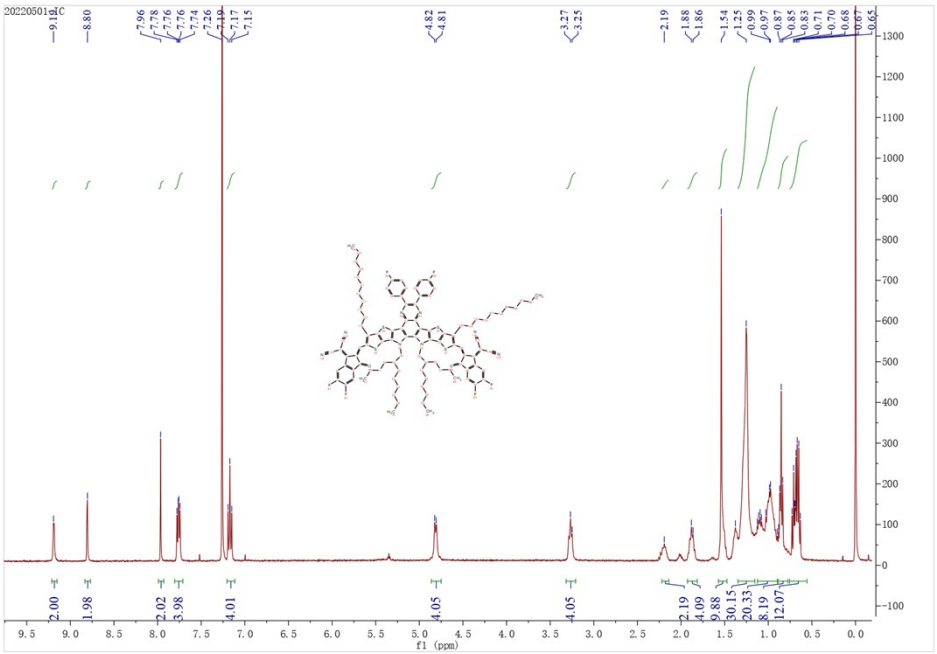

Fig. S26 ^{1}H NMR spectrum of Qx-p-4F in $CDCl_3$.

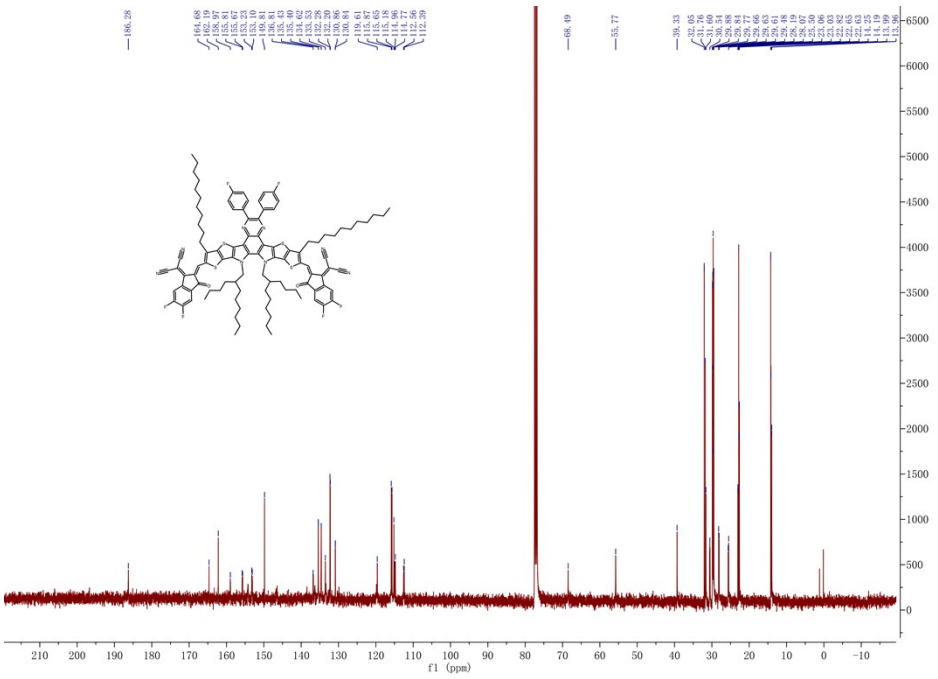

Fig. S27 ^{13}C NMR spectrum of Qx-p-4F in $CDCl_3$.

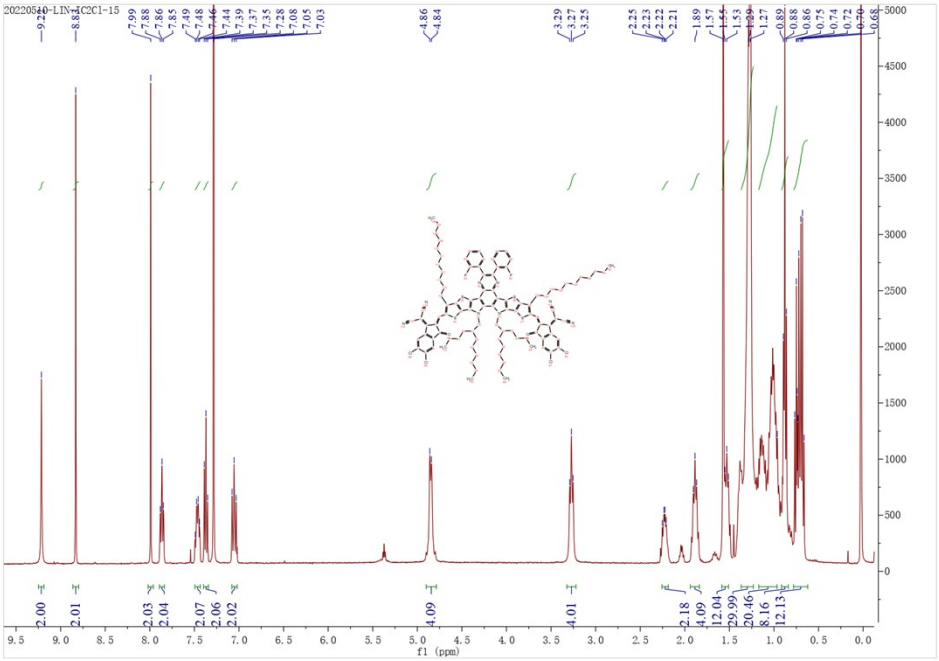

Fig. S28 ^{1}H NMR spectrum of Qx-o-4Cl in $CDCl_3$.

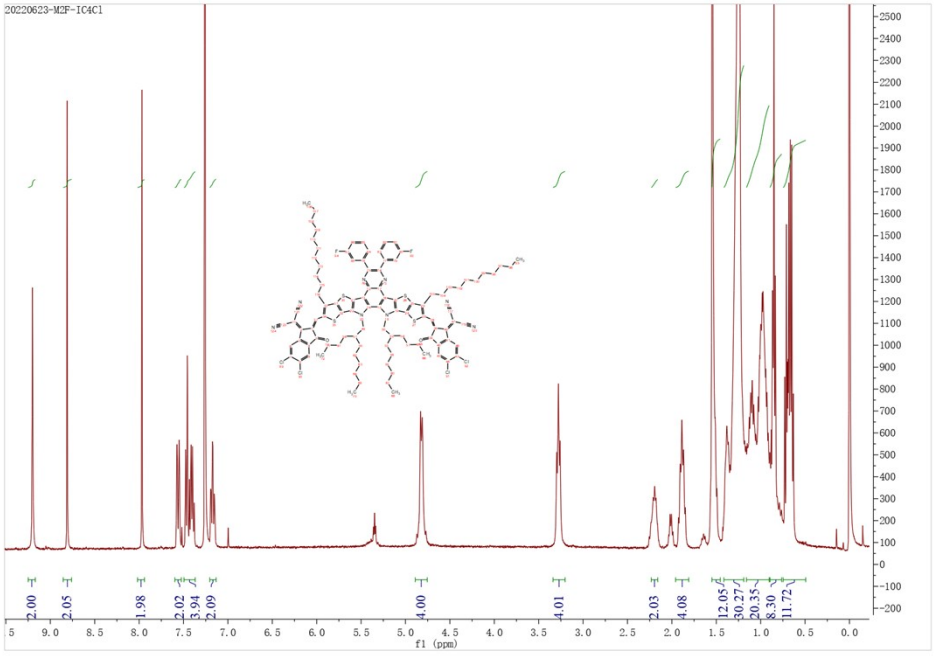

Fig. S29 ^{1}H NMR spectrum of Qx-m-4Cl in $CDCl_3$.

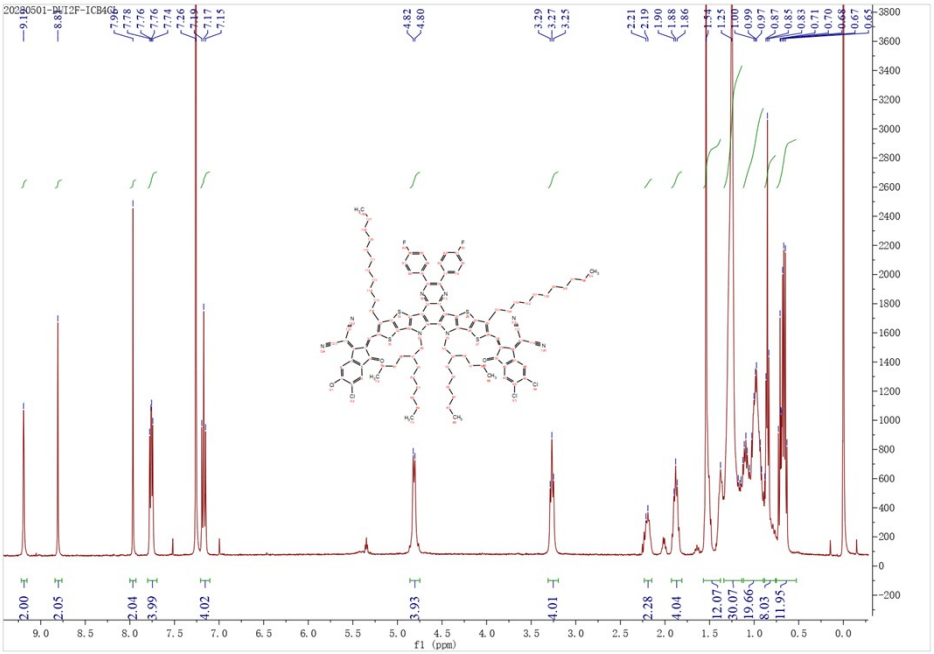

Fig. S30 ^{1}H NMR spectrum of Qx-p-4Cl in $CDCl_3$.

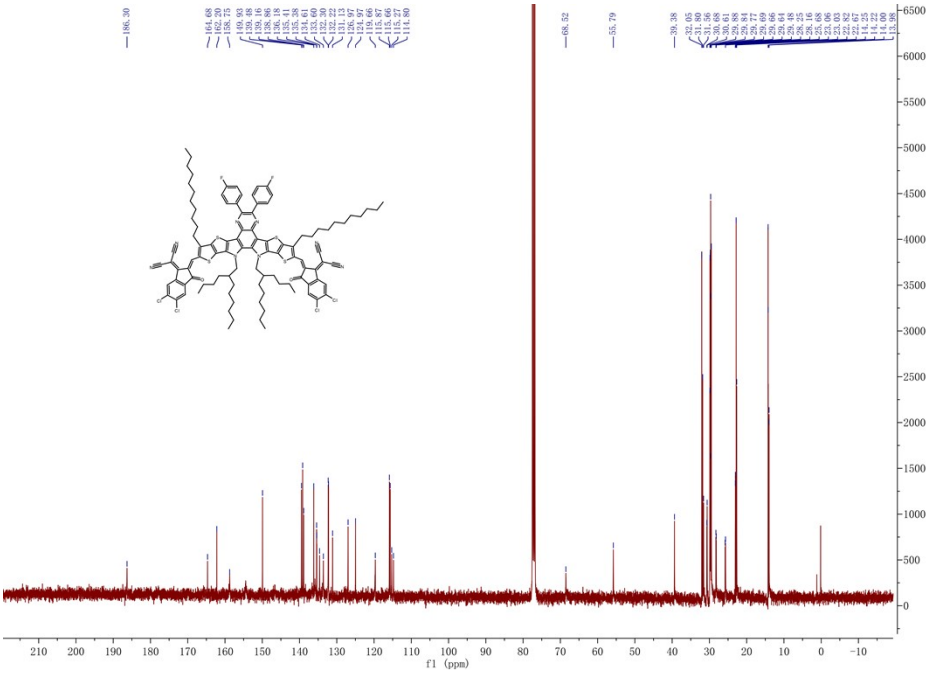

Fig. S31 ^{13}C NMR spectrum of Qx-p-4Cl in $CDCl_3$.

3. Supplementary Tables

Table S1 The detailed optoelectronic properties of the four NFAs

Acceptor	λ_{max}^{sol} [nm]	λ_{max}^{film} [nm]	λ_{onset}^{film} [nm]	E_g^{opt} [eV][a)]	E_{HOMO}/E_{LUMO} [eV]	E_g^{CV} [eV]
Qx-o-4F	741	803	864	1.44	-5.73/-3.92	1.81
Qx-m-4F	737	793	855	1.45	-5.69/-3.82	1.87
Qx-p-4F	739	788	846	1.47	-5.76/-3.91	1.85
Qx-p-4Cl	754	812	878	1.41	-5.65/-3.96	1.69

a) $E_g^{opt} = 1240 / \lambda_{onset}^{film}$; b) $E_g^{CV} = E_{LUMO} - E_{LUMO}$

Table S2 Crystal data and structure refinement for Qx-o-4F (CCDC 2253303) and Qx-m-4F (CCDC 2253302).

Empirical formula	$C_{104}H_{110}F_6N_8O_2S_4$	$C_{104}H_{110}F_6N_8O_2S_4$
Formula weight	1746.31	1746.31
Temperature	180.00(10) K	180.00(10) K
Wavelength	0.71073 Å	0.71073 Å
Crystal system	Monoclinic	Monoclinic
Space group	P 21/c	P 2/n
Unit cell dimensions	a = 22.0344(4) Å b = 27.1704(4) Å c = 38.5671(7) Å a= 90° b= 98.0928(17)° g = 90°	a = 24.3943(8) Å b = 14.1219(4) Å c = 29.0635(8) Å a= 90° b= 103.837(3)° g = 90°
Volume	22859.6(7) $Å^3$	9721.6(5) $Å^3$
Z	8	4
Density (calculated)	1.095 Mg/m^3	1.275 Mg/m^3
Absorption coefficient	0.220 mm^{-1}	0.246 mm^{-1}
F(000)	7928	3928
Crystal size	0.28 x 0.22 x 0.20 mm^3	0.52 x 0.14 x 0.03 mm^3
Theta range for data collection	1.499 to 25.027°.	1.443 to 26.372°.
Index ranges	-26<=h<=24,	-30<=h<=26,

	-32<=k<=32, -38<=l<=45	-17<=k<=17, -19<=l<=36
Reflections collected	111895	56676
Independent reflections	40359 [R(int) = 0.0285]	19888 [R(int) = 0.0290]
Data/restraints/parameters	40359/1371/2429	19888/357/1209
Goodness-of-fit on F^2	1.088	1.061
Final R indices [I>2sigma(I)]	R_1 = 0.1023, wR_2 = 0.2314	R_1 = 0.0812, wR_2 = 0.2083
R indices (all data)	R_1 = 0.1246, wR_2 = 0.2430	R_1 = 0.1044, wR_2 = 0.2236
Largest diff. peak and hole	1.435 and -0.631 e.Å^{-3}	0.690 and -0.702 e.Å^{-3}

Table S3 Device optimization for PM6:Qx-o-4F.

TA [℃]	CN	V_{OC} [V]	J_{SC} [mA cm^{-2}]	FF [%]	PCE [%]
80	0.6	0.925	24.00	72.17	16.03
90	0.6	0.922	23.65	74.65	16.27
100	0.6	0.924	23.07	74.93	15.97
110	0.6	0.924	23.44	73.60	15.95
90	0.5	0.928	24.12	71.62	16.04
90	0.6	0.925	24.06	72.88	16.22
90	**0.8**	**0.931**	**23.87**	**74.36**	**16.52**
90	1.0	0.913	21.98	74.09	14.87

Table S4 Device optimization for PM6:Qx-m-4F.

TA [℃]	CN	V_{OC} [V]	J_{SC} [mA cm^{-2}]	FF [%]	PCE [%]
90	0.6	0.905	23.44	77.31	16.40
100	0.6	0.899	24.00	76.89	16.60
110	0.6	0.899	23.23	77.01	16.09
100	0.5	0.894	23.86	76.00	16.21
100	**0.6**	**0.897**	**24.16**	**76.71**	**16.63**
100	0.8	0.895	23.62	75.57	15.97

Table S5 Device optimization for PM6:Qx-p-4F.

D/A	CN	TA [℃]	V_{OC} [V]	J_{SC} [mA cm^{-2}]	FF [%]	PCE [%]
1:1.1	0.6%	110	0.875	24.51	78.82	16.90
1:1.2	0.6%	110	0.875	24.84	79.34	17.24
1:1.3	0.6%	110	0.876	24.76	78.49	17.02
1:1.2	-	110	0.888	25.52	72.48	16.43
	0.5%	110	0.877	24.43	79.18	16.97
	0.6%	**110**	**0.885**	**24.68**	**79.45**	**17.34**
	0.7%	110	0.875	24.69	78.37	16.94
1:1.2	0.6%	100	0.874	23.95	79.13	16.56
		110	0.884	24.72	79.05	17.27
		120	0.877	24.94	78.11	17.09

Table S6 Device optimization for PM6:Qx-p-4Cl.

D/A	CN	TA [℃]	V_{OC} [V]	J_{SC} [mA cm^{-2}]	FF [%]	PCE [%]
1:1.0	0.6%	110	0.878	24.47	78.82	17.02
1:1.1	0.6%	110	0.881	24.61	79.51	17.39
1:1.2	0.6%	110	0.878	25.51	79.12	17.81
1:1.3	0.6%	110	0.872	25.70	77.72	17.60
	0.5%	110	0.874	25.47	79.60	17.72
1:1.2	0.6%	110	0.870	26.02	79.23	17.93
	0.7%	110	0.873	25.40	79.03	17.77
		100	0.877	25.57	78.61	17.63
1:1.2	**0.6%**	**110**	**0.872**	**26.06**	**78.97**	**17.95**
		120	0.870	25.55	78.65	17.48

Table S7 Photovoltaic parameters of optimized OSCs based on PM6:Qx-m-4Cl and PM6:Qx-o-4Cl.

Active layer	V_{OC} (V)	J_{SC} (mA cm^{-2})	cal. J_{SC} (mA cm^{-2})	FF (%)	PCE[a)] (%)
PM6:Qx-o-4Cl	0.911 (0.910 ± 0.001)	24.36 (24.28 ± 0.15)	23.40	75.66 (75.35 ± 0.35)	16.79 (16.64 ± 0.08)
PM6:Qx-m-4Cl	0.891 (0.891 ± 0.002)	25.11 (24.94 ± 0.18)	24.19	77.15 (76.99 ± 0.43)	17.26 (17.12 ± 0.10)

[a)]The average values and standard deviations obtained from 10 individual devices.

Table S8 The electron and hole mobilities for the neat and blend films.

Blend film	μ_h [10^{-4} cm^2 V^{-1} s^{-1}]	μ_e [10^{-4} cm^2 V^{-1} s^{-1}]	μ_h/μ_e
Qx-o-4F	-	2.32	-
Qx-m-4F	-	2.65	-
Qx-p-4F	-	3.09	-
Qx-p-4Cl	-	4.40	-
PM6:Qx-o-4F	5.72	2.66	2.15
PM6:Qx-m-4F	5.98	2.91	2.05
PM6:Qx-p-4F	6.12	3.30	1.85
PM6:Qx-p-4Cl	6.93	5.04	1.38

Table S9 The π-π stacking (010) parameters of pristine and blend films extracted from GIWAXS.

Film	**Out-of-plane *π-π* stacking (010)**			
	q [$Å^{-1}$]	d-spacing [Å][a)]	FWHM [$Å^{-1}$]	CCL [Å][b)]
PM6	1.68	3.74	0.299	18.91
Qx-o-4F	1.71	3.67	0.343	16.49
Qx-m-4F	1.75	3.59	0.175	32.50
Qx-p-4F	1.67	3.76	0.318	17.78
Qx-p-4Cl	1.71	3.67	0.300	18.85
PM6:Qx-o-4F	1.69	3.72	0.265	21.34
PM6:Qx-m-4F	1.70	3.70	0.271	20.87
PM6:Qx-p-4F	1.70	3.70	0.309	18.30
PM6:Qx-p-4Cl	1.71	3.67	0.255	22.18

[a)]Calculated from the equation: d-spacing=2π/q; [b)]Calculated from the Scherrer equation: CCL=2πK/FWHM, where FWHM is the full-width at half-maximum and K is a shape factor (K=0.9 here).

Table S10 The Detailed GIWAXS parameters of pristine and blend films along the in-plane direction.

Film	In-plane			
	q [Å^{-1}]	d-spacing [Å][a)]	FWHM [Å^{-1}]	CCL [Å][b)]
PM6	0.29	21.67	0.11	51.41
Qx-o-4F	0.39	16.11	0.131	43.17
Qx-m-4F	0.27	23.27	0.045	125.66
	0.52	12.08	0.131	43.17
Qx-p-4F	0.35	17.95	0.071	79.65
	0.44	14.28	0.07	80.78
Qx-p-4Cl	0.38	16.53	0.094	60.16
PM6:Qx-o-4F	0.31	20.27	0.105	53.86
PM6:Qx-m-4F	0.31	20.27	0.087	65.00
PM6:Qx-p-4F	0.3	20.94	0.091	62.14
PM6:Qx-p-4Cl	0.30	20.94	0.089	63.54

[a)]Calculated from the equation: d-spacing=2π/q; [b)]Calculated from the Scherrer equation: CCL=2πK/FWHM, where FWHM is the full-width at half-maximum and K is a shape factor (K=0.9 here).

Table S11 The Detailed GIWAXS parameters of pristine and blend films along the out-of-plane direction.

Film	Out-of-plane			
	q [Å^{-1}]	d-spacing [Å][a)]	FWHM [Å^{-1}]	CCL [Å][b)]
PM6	0.92	6.83	0.143	39.54
	1.29	4.87	0.707	8.00
	1.68	3.74	0.299	18.91
Qx-o-4F	1.47	4.27	0.590	9.58
	1.71	3.67	0.343	16.49
Qx-m-4F	0.51	12.32	0.065	87.00
	0.73	8.61	0.059	95.85
	1.57	4.00	0.242	23.37
	1.75	3.59	0.175	32.50
Qx-p-4F	0.66	9.52	0.093	60.81
	1.31	4.80	0.289	19.57
	1.67	3.76	0.318	17.78
Qx-p-4Cl	1.48	4.25	0.577	9.80
	1.71	3.67	0.300	18.85
PM6:Qx-o-4F	0.50	12.57	0.051	110.88
	0.70	8.98	0.09	62.83
	1.35	4.65	0.470	12.03
	1.69	3.72	0.265	21.34
PM6:Qx-m-4F	0.71	8.85	0.092	61.47
	1.35	4.65	0.573	9.87
	1.70	3.70	0.271	20.87
PM6:Qx-p-4F	1.35	4.65	0.574	9.85
	1.70	3.70	0.309	18.30
PM6:Qx-p-4Cl	1.52	4.13	0.714	7.92
	1.71	3.67	0.255	22.18

[a)]Calculated from the equation: d-spacing=2π/q; [b)]Calculated from the Scherrer equation: CCL=2πK/FWHM, where FWHM is the full-width at half-maximum and K is a shape factor

(K=0.9 here).

Table S12 Detailed energy losses of the four OSCs.

Devices	E_g^{PV} [eV][a)]	V_{OC} [V][b)]	qV_{OC}^{SQ} [eV]	qV_{OC}^{rad} [eV]	E_{loss} [eV]	ΔE_1 [eV]	ΔE_2 [eV]	ΔE_3 [eV]	EQE_{EL}	V_{OC}^{cal} [V]
PM6:Qx-o-4F	1.454	0.932	1.19	1.136	0.522	0.264	0.054	0.202	4.08×10^{-4}	0.934
PM6:Qx-m-4F	1.462	0.913	1.196	1.142	0.549	0.266	0.054	0.229	1.44×10^{-4}	0.913
PM6:Qx-p-4F	1.443	0.883	1.179	1.130	0.560	0.264	0.049	0.246	7.41×10^{-5}	0.884
PM6:Qx-p-4Cl	1.423	0.888	1.16	1.114	0.535	0.262	0.046	0.225	1.52×10^{-4}	0.890

[a)]The photovoltaic bandgap (E_g^{PV}) was extracted from the derivative of EQE curves; [b)]The V_{OC} values of devices were measured without mask.

4. References

1 H. J. Song, T. H. Lee, M. H. Han, J. Y. Lee and D. K. Moon, *Polymer*, 2013, **54**, 1072-1079.

2 Z. Zhou, W. Liu, G. Zhou, M. Zhang, D. Qian, J. Zhang, S. Chen, S. Xu, C. Yang, F. Gao, H. Zhu, F. Liu and X. Zhu, *Adv. Mater.*, 2020, **32**, 1906324.

3 D. Mo, H. Chen, J. Zhou, N. Tang, L. Han, Y. Zhu, P. Chao, H. Lai, Z. Xie and F. He, *J. Mater. Chem. A*, 2020, **8**, 8903-8912.

4 J. Yao, T. Kirchartz, M. S. Vezie, M. A. Faist, W. Gong, Z. He, H. Wu, J. Troughton, T. Watson, D. Bryant and J. Nelson, *Phys. Rev. Appl.*, 2015, **4**, 014020.

5 Y. Wang, D. Qian, Y. Cui, H. Zhang, J. Hou, K. Vandewal, T. Kirchartz and F. Gao, *Adv. Energy Mater.*, 2018, **8**, 1801352.